JACS
JOURNAL OF THE AMERICAN CHEMICAL SOCIETY
Article
pubs.acs.org/JACS

Electrochemical Reduction of CO_2 at Functionalized Au Electrodes

Yuxin Fang and John C. Flake*

Gordon and Mary Cain Department of Chemical Engineering, Louisiana State University, Baton Rouge, Louisiana 70803, United States

Supporting Information

ABSTRACT: Electrochemical reduction of CO_2 provides an opportunity to store renewable energy as fuels with much greater energy densities than batteries. Product selectivity of the reduction reaction is known to be a function of the electrolyte and electrode; however, electrodes modified with functional ligands may offer new methods to control selectivity. Here, we report the electrochemical reduction of CO_2 at functionalized Au surfaces with three thiol-tethered ligands: 2-mercaptopropionic acid, 4-pyridinylethanemercaptan, and cysteamine. Remarkably, Au electrodes modified with 4-pyridinylethanemercaptan show a 2-fold increase in Faradaic efficiency and 3-fold increase in formate production relative to Au foil. Conversely, electrodes with 2-mercaptopropionic acid ligands show nearly 100% Faradaic efficiency toward the hydrogen evolution reaction, while cysteine-modified electrodes show 2-fold increases in both CO and H_2 production. We propose a proton-induced desorption mechanism associated with pK_a of the functionalized ligand as responsible for the dramatic selectivity changes.

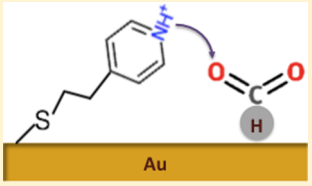

INTRODUCTION

Fuels made via the electrochemical reduction of CO_2 could allow renewable energy storage with several significant advantages over batteries. The specific energy of fuels such as methanol is at least an order of magnitude greater than the best Li-ion batteries on a volumetric basis; further, other fuels (jet fuel, diesel) used in heavy transportation may be synthesized from electrolytically generated alcohols. There are also inherent advantages to storing and transporting energy as liquid fuels relative to batteries such as no self-discharging and relatively low storage costs. Further, it may be possible to operate the entire system in a carbon-neutral process if atmospheric CO_2 is used as the carbon source.[1]

While the electrochemical reduction of CO_2 has been investigated for over a century, the field was reenergized in 1987 by Hori's work showing Cu electrodes were capable of producing significant amounts of methane and ethylene.[2] Since that time, there have been a number of studies aimed at understanding and improving the selectivity and efficiency of CO_2 reduction reactions.

Metals have been thoroughly investigated as heterogeneous electrocatalysts in various forms ranging from polycrystalline foils to nanoparticles.[3−6] Previous works have shown that Au[3,7] and Ag[3] foil electrodes primarily produce CO (with 81−93% and 61−90% Faradaic efficiencies ∼5 mA/cm^2 in 0.5 M $KHCO_3$, respectively). As mentioned, Cu[2,8] electrodes produce hydrocarbons with reasonable Faradaic efficiencies (e.g., CH_4, 29.4%; C_2H_4, 30.1% at 5 mA/cm^2 in 0.1 M $KHCO_3$) but suffer from relatively high overpotential requirements and electrode fouling. Sn electrodes have a relatively high overpotential for the hydrogen evolution reaction (HER) and yield formate as primary product until the formation of SnO_2 deactivates the catalyst.[9] Many consider formate a "dead end";[10] that is, no further C−O bond cleavage in CO_2 or hydrogenation occurs; however, it is important to note that formate is a valuable chemical feedstock and fuel.[11] Other metals such as Pt, Ni, Fe, etc. favor the HER at the potentials required for CO_2 reduction and do not produce any appreciable hydrocarbons.[12]

While Cu electrodes remain the most attractive in terms of hydrocarbon production, the potential to hydrogenate CO intermediates and produce other high-value products such as alcohols appears to be limited with conventional electrodes.[13] There are several potential pathways to mitigate the "scaling relations" [13] that limit CO hydrogenation including the use of nanoscale electrodes (exposing atomically precise sites[5,14]), alloys (shifting the d-band center energy level[15−17]), surface ligands (forming hydrogen-bond like interactions for intermediates[18]) to stabilize the adsorption of key intermediates (COOH* or CO*), and/or electrode mediators (i.e., those capable of capturing CO_2).[19]

It is important to note that nature uses all of the aforementioned tools to selectively convert CO_2 to a wonderful variety of products.[20,21] Likewise, there have been some studies showing electrolyte additives such as pyridine or the use of molecular catalysts like pterins lead to the formation of alcohols or other higher value hydrocarbons.[22] Bocarsly et al. showed Faradaic efficiencies up to 30% for CH_3OH at 40 μA/cm^2 on Pd/Pt using 10 mM pyridine additives to the electrolyte.[23] The pyridinium ($pyrH^+$) was proposed as the active homogeneous catalysts until later studies suggested that the pyridinium radical (pyrH*) functioned as one-electron charge-transfer mediator for the production of methanol at the electrode surface.[24,25] Further pyridine substituted groups yielded up to 30% Faradaic efficiency to CH_3OH production; however, these results were generated at relatively low current densities (∼50 μA/cm^2).[26] Likewise, Dyer et al. studied the use of pterins, namely mercaptopteridine (PTE), as molecular catalysts in 0.1 M KCl at glassy carbon

Received: October 21, 2016
Published: February 9, 2017

DOI: 10.1021/jacs.6b11023
J. Am. Chem. Soc. 2017, 139, 3399−3405

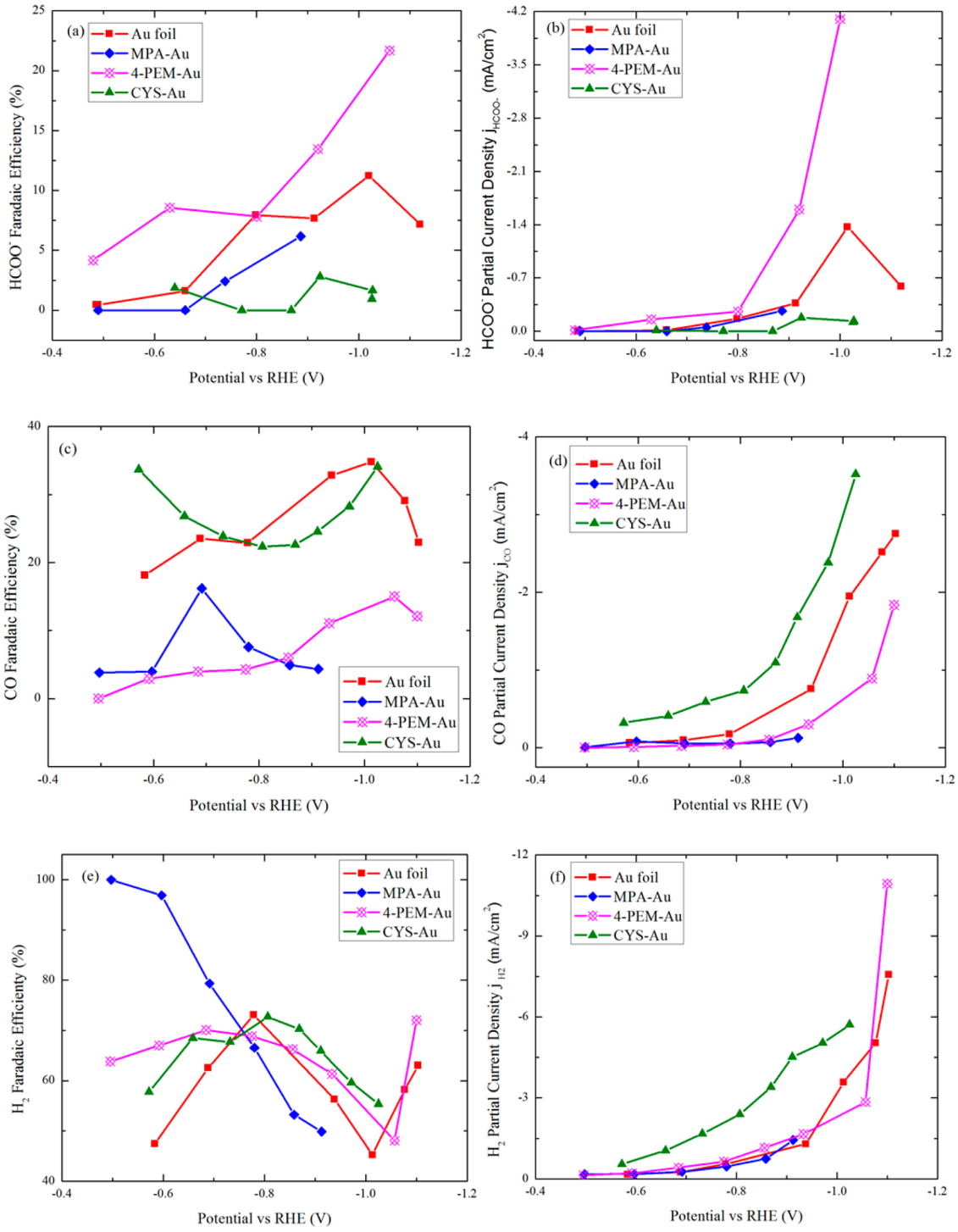

Figure 1. Comparison of partial current density and Faradaic efficiency (FE) for thiolate ligand on polycrystalline Au and pure polycrystalline Au: (a) FE of formate formation (±2.5% at 95% confidence level (CL)), (b) FE of CO formation (±6.2% at 95% CL), (c) FE of H_2 formation (±25% at 95% CL); (d) partial current density of formate formation; (e) partial current density of CO formation, and (f) partial current density of H_2 formation.

electrodes that yielded 10−24% CH_3OH at 100 $\mu A/cm^2$ which was similarly attributed to the electron-transfer ability of pterin.[22]

In this work we focus on CO_2 reduction and hydrogenation via monolayers of thiol-tethered functional ligands on Au electrodes. Au was chosen as the substrate since it is noble and forms strong S−Au covalent bonds.[27] Three ligands, 2-mercaptopropionic acid (MPA), 4-pyridylethylmercaptan (4-PEM), and cystemine (CYS), were selected as the functional ligands because of their pK_a range from low to high (3.7, 5.2, 9.25). The gas and liquid products at the surface-modified electrodes are analyzed as well as the stability of the ligand-modified surfaces.

RESULTS AND DISCUSSION

Product Analysis. Figure 1 shows the potential-dependent product distribution (expressed in Faradaic efficiency for selectivity and partial current density for yield of each compound) from CO_2 reduction on functionalized Au and untreated Au surfaces. The primary products including formate,

DOI: 10.1021/jacs.6b11023
J. Am. Chem. Soc. 2017, 139, 3399−3405

CO, and H_2 were characterized by NMR and GC analysis. Their potential-dependent yield behavior and Faradaic efficiencies are discussed in the following sections.

Relative to untreated Au foil, MPA-modified Au electrodes produced hydrogen as a primary product (Faradaic efficiency near 100%) in the low overpotential range (> −0.8 V vs RHE) while CO evolution was suppressed. The greatest observed Faradaic efficiency for CO evolution is less than 20% which is roughly half of that on untreated Au. Likewise, the formate production is reduced by approximately half when MPA is tethered to the electrode. The potential range investigated using MPA-modified Au was limited to > −0.94 V vs RHE, due to desorption of surface ligands at high overpotentials which is discussed later.

Remarkably, the 4-PEM-modified electrodes produced approximately 3 times more formate (−4.1 mA/cm^2) relative to the optimal observed on Au foil (−1.37 mA/cm^2). In terms of the Faradaic efficiency for the reduction to formate, a maxima of 21% with Au/4-PEM electrode (at −1.00 V vs RHE) was achieved compared with 11% on Au surfaces (at −1.01 V vs RHE). On the other hand, the CO partial current was suppressed on the same electrode by at least half relative to Au over the entire potential range of interest. It is interesting to note that the 4-PEM-modified Au shows selectivity toward the HER at low potentials (−0.5 to −0.7 V vs RHE), then CO_2 reduction increases in the potential range from −0.7 to −1.1 V vs RHE. Electrolysis in N_2 saturated electrolyte experiments were employed to rule out the possibility of thiolate decomposition into formate.

As for the CYS-functionalized Au electrode, formate production was suppressed relative to Au within the entire potential range of interest. Although the selectivities of CO and H_2 were similar to those at Au foil, the electrode was significantly more active (i.e., the partial current density j_{CO} and j_{H_2} were increased by more than 2-fold).

Table 1 summarizes the onset potentials for HER and CO_2 reduction on (functionalized) Au substrates. On the MPA-functionalized Au, onset potentials for HER and CO_2 reduction were both shifted anodically (by +10 and +100 mV, respectively). With the 4-PEM-functionalized Au electrode, the HER onset potential was shifted cathodically (−50 mV), and the onset potential of CO_2 reduction was shifted anodically (+30 mV). On the CYS-functionalized Au, both onset potentials were shifted anodically (+90 and +70 mV, respectively). The enhancement in Faradaic selectivity toward HER on MPA- and 4-PEM-functionalized Au may be associated with the decreased onset potential differences ($E_{HER}^0 - E_{CO_2}^0$) following ligand modification. The correlation between HER selectivity change (S_1/S_2) and onset potential difference may be expressed in a Butler−Volmer relationship. For example, eq 1a shows yields in terms of the reactant concentrations C_H and C_C, transfer coefficient α, normalized Faraday's constant f, and time t (see SI, eqs S1−S5).[28] Assuming similar concentrations of H^+ and CO_2, eq 1a can be simplified into eq 2; thus, the decrease in the difference of onset potentials results in increased HER selectivity. On CYS-functionalized Au, the onset potential shifts anodically for both reactions so the product selectivity remains roughly equivalent to the untreated Au electrode.

Table 1. Onset Potentials of HER and CO_2 Reduction and Their Difference on (Functionalized) Au Surfaces

surface	HER (V vs RHE)	CO_2 reduction (V vs RHE)	$V_{HER} - V_{CO_2RR}$ (mV)
Au	−0.30	−0.42	120
MPA-Au	−0.29	−0.32	30
4-PEM-Au	−0.35	−0.39	40
CYS-Au	−0.21	−0.35	140

$$\frac{S_1}{S_2} = \frac{C_{H1}(0,t)C_{C2}(0,t)}{C_{H2}(0,t)C_{C1}(0,t)} e^{-2\alpha f[(E^0_{2,HER}-E^0_{2,CO_2})-(E^0_{1,HER}-E^0_{1,CO_2})]} \quad (1a)$$

$$\frac{S_1}{S_2} = \frac{R_1}{R_2} e^{-2\alpha f[(E^0_{2,HER}-E^0_{2,CO_2})-(E^0_{1,HER}-E^0_{1,CO_2})]} \quad (1b)$$

$$\frac{S_1}{S_2} = e^{-2\alpha f[(E^0_{2,HER}-E^0_{2,CO_2})-(E^0_{1,HER}-E^0_{1,CO_2})]} \quad (2)$$

The dramatic differences in HER selectivity on 2-MPA-Au and 4-PEM-Au at lower potentials (with approximately same onset potential differences) suggest the surface concentration ratio R ($R = C_H/C_C$) must be different. Recent studies on the role of cations by Bell et al. have suggested proton donation from the dissociation of hydrated cations buffers the local electrolyte once the pK_a of hydrated cations is lower than local pH.[29] Similar behavior was also observed by Kenis et al.'s study on the effect of hydrated cations on the current density of CO evolution.[30] The pK_a values of the functional groups are summarized in Table 2.

Table 2. pK_a Values of Thiolate Ligands

ligand	pK_a
2-mercaptoproponic acid (2-MPA)	3.7 (ref 31)
4-pyridylethylmercaptan (4-PEM)	5.2 (ref 26)
cysteamine (CYS)	9.25 (ref 32)

Thus, the higher $R_{(MPA)}$ may be attributed to the lower pK_a of surface ligand. The HER selectivity at higher potentials may also be attributed to the dominant surface species. As shown in the following section, the deprotonated MPA is the main species on MPA-Au (shown in the stability analysis with IR spectrum). Here, the lower pK_a makes MPA both a good proton donor and poor acceptor; thus, the surface concentration ratio of H^+ to CO_2 is lower at high potential. The selectivity shift from CO and current density enhancement associated with formate evolution is further discussed in later sections.

Stability Analysis. One important concern associated with the electrochemical reduction of CO_2 in the presence of functionalized surfaces is the stability of the ligand at the potentials required to reduce CO_2. Several studies have shown the cathodic desorption and dissolution of alkanethiolates on gold;[33,34] however, many thiolates are considered stable at cathodic potentials.[35] More recent *in situ* work with sum frequency generation vibrational spectroscopy by Badeli et al.[27] shows that octadecanethiol ligands remain at the surface even at high cathodic potentials owing to the van der Waals interaction between alkyl chain and the low solubility in aqueous solution. Aromatic thiolates are particularly stable as the aromatic group appears to enhance surface bonding.[36] Here we carried out the *ex situ* ATR-IR experiments to study the stability of ligands on Au foil.

2-Mercaptopropionic Acid (MPA). Figure 2 compares the ATR-IR spectrum between freshly prepared MPA-Au sample along with the same sample post-electrolysis at −0.94 V vs RHE

DOI: 10.1021/jacs.6b11023
J. Am. Chem. Soc. 2017, 139, 3399−3405

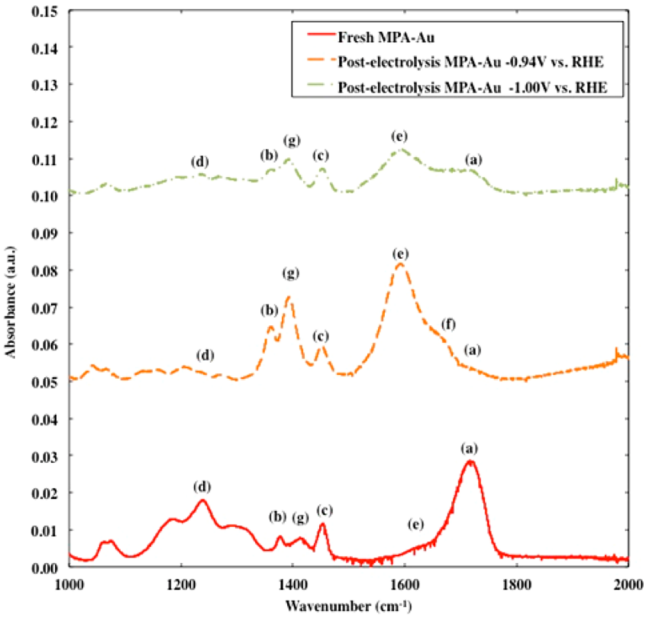

Figure 2. Comparison of ATR-IR spectra for MPA SAM on Au: (red) freshly prepared, (orange) post-electrolysis at −0.94 V vs RHE, and (green) post-electrolysis at −1.00 V vs RHE.

and post-electrolysis at −1.00 V vs RHE (solution-phase thiols spectra are available in the SI). In the freshly prepared electrode spectra, vibrations at 1723 cm^{-1} (a) correspond to the C═O stretching of the COOH group. The symmetric and asymmetric stretching signals of the $-CH_3$ group showed up at 1372 cm^{-1} (b) and 1449 cm^{-1} (c). The C−C stretching is also observed at 1241 cm^{-1} (d).[37,38] The slight shoulder at 1607 cm^{-1} (e) and the small peak at 1421 cm^{-1} (g) correspond to the asymmetric and symmetric stretching of $-COO^-$, respectively.[38] On the spectrum of the post-electrolysis (−0.94 V vs RHE) MPA-modified Au sample, the asymmetric stretching vibration at 1583 cm^{-1} (e) with a shoulder at 1662 cm^{-1} (f) indicates the presence of the deprotonated COO^- group and COOH group, respectively. The rise of peak (g), coupling with peak (e) indicates that deprotonated ligand species dominate the surface during/after the electrolysis. The vibrations of the CH_3 group and the C−C bond remain similar in pre- and post-electrolysis samples. Slight shifts in wavenumbers indicate that the change in configuration of the monolayer results in stronger interaction between the Au surface and the functional group. However, at more negative potentials (−1.00 V vs RHE), decreased absorbance associated with $-CH_3$ group and COO^- group suggests the lower concentration of surface ligand. This suggests the potential window for MPA to remain on the surface is below −0.94 V vs RHE.

4-Pyridylethylmercaptan (4-PEM). Figure 3 presents the comparison between the freshly prepared 4-PEM-Au spectra and the post-reaction spectra at −1.04 V vs RHE for the sample. The bands at 1606 cm^{-1} (a), 1564 cm^{-1} (b), and 1521 cm^{-1} (c)[38,39] characterizing the ring structures in pyridine and 780 cm^{-1} (f) and 850 cm^{-1} (e) characterizing C−H deformation vibration present in both spectra.[38,40] The vibration (d) was shifted from 1506 to 1484 cm^{-1}, indicating the presence of protonated pyridine species on the surface.[39] This indicates that the 4-PEM remains intact at −1.04 V vs RHE within time of electrolysis for the product analysis and further that the pyridinium is the main functioning ligand in the reactions. The presence of protonated

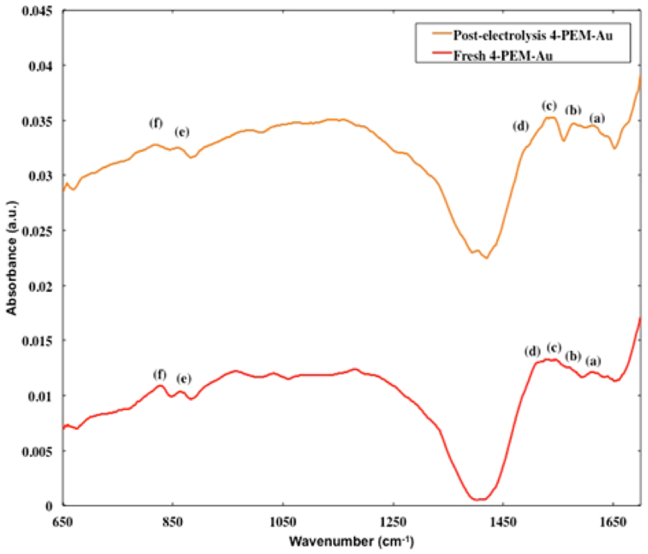

Figure 3. Comparison of ATR-IR spectra for 4-PEM SAM on Au: (red) freshly prepared and (orange) post-electrolysis at −1.04 V vs RHE.

species during/after further supports the notion of ligand participation in proton transfer reactions.

Cysteamine (CYS). Figure 4 shows the comparison between the spectra of the freshly prepared CYS-Au surface and the

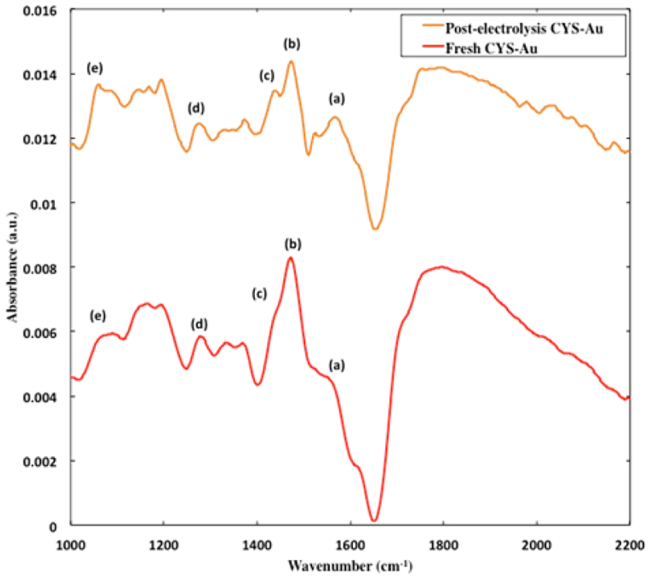

Figure 4. Comparison of ATR-IR spectra for CYS SAM on Au: (red) freshly prepared and (orange) post-electrolysis at −1.1 V vs RHE.

spectra from the same electrode post-electrolysis. These spectra show absorbance peaks at 1550 cm^{-1} (a), 1465 cm^{-1} (b), 1430 cm^{-1}(c), 1272 cm^{-1} (d), and 1064 cm^{-1} (e), which correspond to the N−H bonds' bending vibrations, CH_2 deformation, CH_2−S wagging, and C−N stretching, respectively.[38,41] Note, the solution-phase ligand FTIR spectra may be found in the SI. The red shifts indicate the strong interactions between the surface and the ligand. The presence of the absorption peaks in both spectra confirms the stability of cysteamine on the Au surfaces within the potential range of interest.

Mechanism. Clearly, ligand modification of Au electrodes influences product selectivity of the CO_2 reduction reaction.

DOI: 10.1021/jacs.6b11023
J. Am. Chem. Soc. 2017, 139, 3399−3405

Scheme 1. Proposed Formate Formation Mechanism at 4-Pyridylethylmercaptan-Modified Au Surface

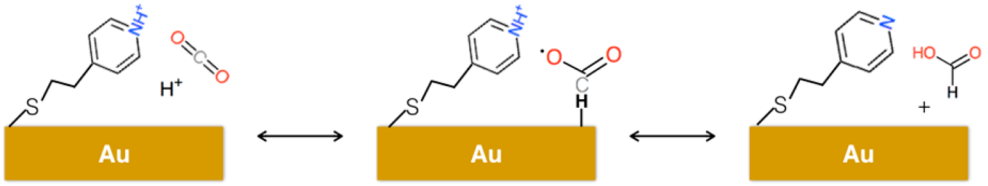

Based on these results, the nature of the shifted selectivity likely originates from the separation of proton- and electron-transfer reactions enabled by the ligand. For example, consider the directed proton transfer behavior of enzymes involved in proton-coupled electron-transfer (PCET) reactions.[42−44] Nocera et al. showed that enzymes are capable of disentangling proton transfer and electron transfer and allowing transfer coordinates on highly different length scales. In fact several studies have explored the potential of "wiring" enzymes to combine the selectivity of the natural catalysts with the advantages of externally driven cells.[45−47] While there are limitations related to the wiring of enzymes and stability concerns, there are a number of works showing that functionalized electrodes, such as those considered here, are stable in the potential range needed for electrochemical reduction reactions.[18,48,49] Given the wonderful selectivity of natural catalysts, it is likely that similar directed proton transfer reactions are possible at ligand-functionalized electrodes, especially at moderate potentials.

The 3-fold increase observed in formate production when Au electrodes are functionalized with 4-PEM is remarkable. Given the presence of pyridine functional group, previous results on pyridine/Pt systems may provide some mechanistic insights. Bocarsly et al. reported the production of CH_3OH (11−39% Faradaic efficiency) and HCOOH (7−16% Faradaic efficiency) with Pt/Pd electrodes in the presence of 10 mM pyridine and its substituted derivatives in the supporting electrolyte.[23,26] Pt was reported as HER dominant (~95% Faradaic efficiency) electrocatalysts, and Pd mainly yields CO formation.[12] While the current density with the 10 mM pyridine-dosed electrolysis was relatively low (50 $\mu A/cm^2$) compared to this work (0.2−15 mA/cm^2); pyridine appears to have a strong influence in the CO_2 reduction selectivity. However, the question of whether a surface or solution-phase pyridinium is involved is unknown.

Initial work by Bocarsly et al. analyzed the data from cyclic voltammetry and proposed a mechanism[24] that proceeds with pyrH* as co-catalyst based on Gaussian calculations: a $1e^-$ reduction of the $pyrH^+$ to pyrH* that reacts with CO_2 and forms a CO_2-pyrH radical carbamate with inner-sphere interaction, and another surface-adsorbed H-atom reacted with the surface-adsorbed carbamate to yield formic acid. In that mechanism, further proton shuttling to formate yields methanol. Later work considering acidity constants for $pyrH^+$ and pyrH* by Keith and Carter showed the unfavorable deprotonation step for pyrH* since its pK_a was calculated as ~27.[50] Instead, they proposed a surface mechanism[51,52] using first-principles quantum chemistry where the surface bound dihydropyridine (DHP) is the co-catalyst that takes hydride from Pt and transfers the hydride and proton to the CO_2 to yield formate.

In another study of the functional role of $pyrH^+$ during aqueous CO_2 electrochemical reduction, Batista et al. proposed an alternate proton-coupled hydride-transfer mechanism.[53] The $1e^-$ reduction of $pyrH^+$ produced hydride on Pt surface. CO_2 is susceptible to a $1e^-$ reduction by the surface hydride coupled with another proton from $pyrH^+$. In our work, the structure of the tethered 4-PEM likely prohibits formation of DHP since the C-atom para to N is fully bonded and does not undergo hydrogenation. Also, the thiol-tether and electron-transfer requirements[54] make the pyridinium radical formation unlikely since the electron-transfer rate constant decays exponentially with the increase in donor−acceptor distance (Au and N). The electron-transfer limitations also apply to Batista's PCET model where the surface hydride is replenished by the reduction of $pyrH^+$.

Here, we propose a modified formate production mechanism (depicted in Scheme 1) on 4-PEM-modified Au electrodes. The first proton from aqueous solution is reduced and forms an H-atom adsorbed on Au (step 1a). Note the moderate pK_a,

Step 1a:

Step 1b:

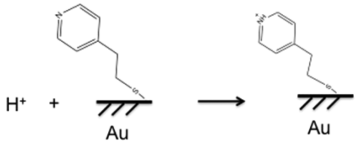

Step 2:

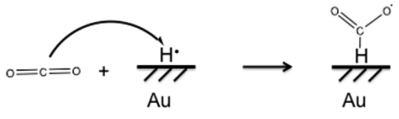

Step 3a:

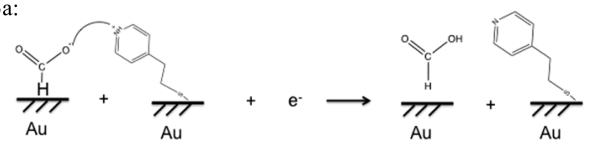

Step 3b:

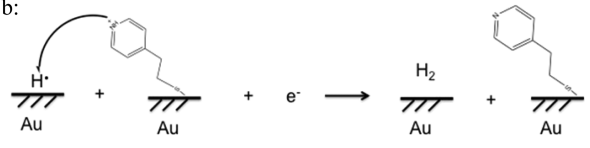

suggesting that the surface is not dominated by protons from the $pyrH^+$. A $2e^-$ transfer to hyride is not plausible since the hydride-dominated surface would result in HER, assuming sufficient protons are available from solution. The electrophilic attack of CO_2 to the adsorbed H yields HCO_2* (step 2).[55]

Compared with Au foil, the slightly higher surface concentration of H^+ (5.2 for 4-PEM versus 6.8 in 0.1 M

DOI: 10.1021/jacs.6b11023
J. Am. Chem. Soc. 2017, 139, 3399−3405

$KHCO_3$) decreases the probability of first electron transfer to CO_2^- and forms the −COOH with the proton from the solution which is the expected path to the CO evolution.[6,55−57] Thus, a HCO_2* intermediate after the first pair of proton−electron transfer steps is likely a key step toward the production of formate. Previous simulation studies by Norskov et al. have shown strong correlations between HCO_2* and $HCOO^-$.[55] Thus, a slight selectivity shift between CO and formate is probable. Next, the tethered $pyrH^+$ in the thiolate group transfers a proton to the nearby oxygen of the HCO_2* coupled with $1e^-$ transfer from the surface (Step 3a). The enhanced HER observed at lower potentials also supports this proton-induced desorption mechanism (Step 3b). The protonated $pyrH^+$ is replenished with proton source from the electrolyte (Step 1b).

According to this mechanism, we propose that the proton-donating ability (pK_a) of the ligand correlates with CO_2 reduction to formate and H_2 yields as observed on functionalized Au electrodes. Ligands with low pK_a values such as 2-MPA, facile proton donation favors the HER through Step 3b. Ligands with high pK_a, such as CYS result in diminished deprotonation as well as Step 3b. Thus, the product selectivity is virtually unchanged relative to untreated Au electrodes. The 2-fold enhancement in partial current density observed with CYS is likely the result of the amine's ability[58] to complex CO_2 near the surface. The intermediate pK_a of 4-PEM (= 5.2) facilitates the proton transfer to CO_2 in a way that yields formate.

CONCLUSION

Au electrodes functionalized with monolayers of thiol-tethered ligands were evaluated for their ability alter the selectively of CO_2 reduction reaction. A 2-fold increase in Faradaic efficiency and 3-fold increase in formate yield were observed with the 4-PEM-modified Au compared to the best results with untreated Au. MPA-modified Au electrodes favored only the HER, and CYS-modified Au resulted in increased CO and H_2 production with virtually no changes in selectivity. A proton-induced desorption mechanism is proposed to account for the remarkable increase in formate production on 4-PEM-modified Au electrodes. The inability of the CYS- and MPA-modified electrodes to yield significant amounts of formate is believed to be associated with the pK_a of the surface-tethered functional group. At a more fundamental level, this ligand-mediated proton-transfer step demonstrates the potential for improved selectivity via "directed hydrogenation" reactions.

EXPERIMENTAL SECTION

Electrode Preparation. Au foil electrodes (99.99%, ESPI) were rinsed with deionized water (MegaPure system) and used as working electrode. The functionalized electrodes were prepared as follows: Au metal foils were rinsed in deionized (DI) water followed by the solvent of ligands copiously before immersion into the 20 mM 2-mercaptopropionic acid (Sigma-Aldrich, 95%) ethanolic (Pharmco-Aaper, ACS) solution, 20 mM cysteamine (Sigma-Aldrich 95%) aqueous solution, and 20 mM 4-pyridylethylmercaptan (Aldrich) methanolic (EMD, ACS) solution for 10, 10, and 5 min, respectively. Previous studies have shown short immersion times are sufficient for the chemical adsorption of thiolate at μM thiol solution concentration to reach a packing density at 4.47×10^{-10} mol/cm^2.[59,60] The formation of thiol layer takes less time at higher concentration solution.[61] A well ordered pyridinylthiol monolayer on Au was studied after 5 min immersion.[40,62] The thiolate-modified electrodes were then rinsed with solvent of the solution followed by DI water to remove the non-chemisorbed thiol and solvent molecule. A fresh electrode was prepared at each potential to ensure the consistency of the experiments.

Electrochemical Methods. Electrochemical experiments were carried out using a H-type electrochemical cell separated by Nafion membrane (FuelCellsEtc) to prevent the CO_2 reduction product from being reoxidized. The (functionalized) Au foil served as the cathode, while the Pt wire served as the auxiliary electrode. The potential was measured with respect to an Ag/AgCl (saturated with 3 M NaCl) reference electrode (BASi, RE-5B) by a PAR model 263A potentiostat/galvanostat followed by the manual correction of uncompensated resistance. The potentials in this study were reported versus RHE with the conversion E(vs RHE)= E(vs Ag/AgCl) + 0.197 + 0.059*pH. The current density was obtained by normalized with the Au geometric surface area.

Cyclic voltammetry (CV) was performed with the scanning rate at 10 mV/s from 0.2 to −2.0 V vs Ag/AgCl in 0.1 M $KHCO_3$ (Sigma-Aldrich, ACS reagent) as supporting electrolyte. The solution was bubbled with N_2 (Air Liquide, UHP) for 30 min to produce a purged solution of pH 9 for HER reaction studies. For the CO_2 (Air Liquide, 99.99%) reduction reaction, it was purged with N_2 for 20 min to remove O_2, and then CO_2 was bubbled into the solution for 30 min, producing a saturated solution with pH 6.8. The onset potentials for HER and CO_2 RR were determined from Tafel plots of CVs in N_2-saturated electrolyte and CO_2-saturated electrolyte, respectively[6364] (see example in SI).

For the gaseous product analyses, CO_2 was bubbled continuously into the electrochemical cell at a flow rate of 40 mL/min and a pressure of 1 atm, while potentials were applied by stepping to desired potential and held for 15 min. At the 15 min interval, the gas products (CO and H_2) in the effluent from the electrolysis were auto-sampled to the gas chromatograph (Shimadzu, GC 2014) that equipped with FID and TCD detectors. The concentrations of individual gases were analyzed to give the production rate (expressed in partial current density, j_i) and Faradaic selectivity.

The liquid products analyses on the 30 min bulk electrolysis electrolyte were carried out with an VNMS 700 spectrometer with an excitation sculpting pulse technique for water suppression as described by Jaramillo et al.;[8] 10 mM DMSO was used as the reference peak. The 1D ^{1}H NMR data were processed with MestReNova. Considering the alcoholic thiol solution used here may result in false reading in higher hydrocarbon product, formate is the only liquid product discussed here.

Surface Self-Assembled Monolayer (SAM) Characterization. ATR-IR infrared spectra were measured on a smart-ITR diamond assembled Nicolet 6700 FTIR spectrometer with a nitrogen-cooled narrow-band MCT detector. Spectra were recorded for the fresh prepared electrode before any electro-reduction. The same chronoamperometry experiments for NMR electrolysis were then performed in the same two-compartment electrochemical cell at various controlled potentials until −1.1 V vs RHE, the highest overpotential applied for the product analysis. Spectra were taken after each potential step. Interferograms were recorded at a resolution of 0.5 cm^{-1} and 256 scans. Comparison with previous reported literature excluded the possibility that the absorption peaks are from the potassium bicarbonate.[65]

ASSOCIATED CONTENT

Supporting Information

The Supporting Information is available free of charge on the ACS Publications website at DOI: 10.1021/jacs.6b11023.

Statistics, onset potential, solution-phase thiol IR spectra, and AFM data (PDF)

AUTHOR INFORMATION

Corresponding Author

*johnflake@lsu.edu

ORCID

John C. Flake: 0000-0002-9187-3143

Notes

The authors declare no competing financial interest.

DOI: 10.1021/jacs.6b11023
J. Am. Chem. Soc. 2017, 139, 3399−3405

■ ACKNOWLEDGMENTS

This work was supported by the U.S. National Science Foundation under Grant No. CBET-1438385. The authors would like to thank Dr. Thomas Weldeghiorghis in the Louisiana State University Chemistry Department for his help with the NMR analysis.

■ REFERENCES

(1) Jhong, H.-R. M.; Ma, S.; Kenis, P. J. A. *Curr. Opin. Chem. Eng.* **2013**, *2*, 191−199.
(2) Hori, Y.; Murata, A.; Takahashi, R. *J. Chem. Soc., Faraday Trans. 1* **1989**, *85*, 2309−2326.
(3) Hori, Y.; Kikuchi, K.; Suzuki, S. *Chem. Lett.* **1985**, *14*, 1695−1698.
(4) Hori, Y.; Murata, A.; Takahashi, R.; Suzuki, S. *Chem. Lett.* **1987**, *16*, 1665−1668.
(5) Kauffman, D. R.; Alfonso, D.; Matranga, C.; Qian, H.; Jin, R. *J. Am. Chem. Soc.* **2012**, *134*, 10237−10243.
(6) Zhu, W.; Michalsky, R.; Metin, Ö.; Lv, H.; Guo, S.; Wright, C. J.; Sun, X.; Peterson, A. A.; Sun, S. *J. Am. Chem. Soc.* **2013**, *135*, 16833−16836.
(7) Hori, Y.; Murata, A.; Kikuchi, K; Suzuki, S. *J. Chem. Soc., Chem. Commun.* **1987**, 728−729.
(8) Kuhl, K. P.; Cave, E. R.; Abram, D. N.; Jaramillo, T. F. *Energy Environ. Sci.* **2012**, *5*, 7050−7059.
(9) Anawati; Frankel, G. S.; Agarwal, A.; Sridhar, N. *Electrochim. Acta* **2014**, *133*, 188−196.
(10) Vesselli, E.; Rizzi, M.; De Rogatis, L.; Ding, X.; Baraldi, A.; Comelli, G.; Savio, L.; Vattuone, L.; Rocca, M.; Fornasiero, P.; Baldereschi, A.; Peressi, M. *J. Phys. Chem. Lett.* **2010**, *1*, 402−406.
(11) Holladay, J.; Bozell, J.; White, J.; Johnson, D. *DOE Report PNNL* **2007**, 16983.
(12) Hori, Y. Electrochemical CO_2 Reduction on Metal Electrodes. In *Modern Aspects of Electrochemistry*;Vayenas, C., White, R., Gamboa-Aldeco, M., Eds.; Springer: New York, 2008; Vol. *42*, pp 89−189.
(13) Shi, C.; Hansen, H. A.; Lausche, A. C.; Norskov, J. K. *Phys. Chem. Chem. Phys.* **2014**, *16*, 4720−4727.
(14) Manthiram, K.; Beberwyck, B. J.; Alivisatos, A. P. *J. Am. Chem. Soc.* **2014**, *136*, 13319−13325.
(15) Bligaard, T.; Nørskov, J. K. *Electrochim. Acta* **2007**, *52*, 5512−5516.
(16) Christophe, J.; Doneux, T.; Buess-Herman, C. *Electrocatalysis* **2012**, *3*, 139−146.
(17) Watanabe, M.; Shibata, M.; Kato, A.; Azuma, M.; Sakata, T. *J. Electrochem. Soc.* **1991**, *138*, 3382−3389.
(18) Xie, M.; Xia, B. Y.; Li, Y.; Yan, Y.; Yang, Y.; Sun, Q.; Chan, S. H.; Fisher, A. C.; Wang, X. *Energy Environ. Sci.* **2016**, *9*, 1687−1695.
(19) Ogura, K.; Fujita, M. *J. Mol. Catal.* **1987**, *41*, 303−311.
(20) Rakowski Dubois, M.; Dubois, D. L. *Acc. Chem. Res.* **2009**, *42*, 1974−1982.
(21) Jeoung, J.-H.; Dobbek, H. *Science* **2007**, *318*, 1461−1464.
(22) Xiang, D.; Magana, D.; Dyer, R. B. *J. Am. Chem. Soc.* **2014**, *136*, 14007−14010.
(23) Seshadri, G.; Lin, C.; Bocarsly, A. B. *J. Electroanal. Chem.* **1994**, *372*, 145−150.
(24) Barton Cole, E.; Lakkaraju, P. S.; Rampulla, D. M.; Morris, A. J.; Abelev, E.; Bocarsly, A. B. *J. Am. Chem. Soc.* **2010**, *132*, 11539−11551.
(25) Morris, A. J.; McGibbon, R. T.; Bocarsly, A. B. *ChemSusChem* **2011**, *4*, 191−196.
(26) Barton Cole, E.; Baruch, M.; L'Esperance, R.; Kelly, M.; Lakkaraju, P.; Zeitler, E.; Bocarsly, A. *Top. Catal.* **2015**, *58*, 15−22.
(27) Jacob, J. D. C.; Lee, T. R.; Baldelli, S. *J. Phys. Chem. C* **2014**, *118*, 29126−29134.
(28) Bard, A. J.; Faulkner, L. R.; Leddy, J.; Zoski, C. G. *Electrochemical methods: fundamentals and applications*; Wiley: New York, 1980; Vol. *2*.
(29) Singh, M. R.; Kwon, Y.; Lum, Y.; Ager, J. W.; Bell, A. T. *J. Am. Chem. Soc.* **2016**, *138*, 13006−13012.
(30) Thorson, M. R.; Siil, K. I.; Kenis, P. J. A. *J. Electrochem. Soc.* **2013**, *160*, F69−F74.
(31) Cannan, R. K.; Knight, B. C. J. G. *Biochem. J.* **1927**, *21*, 1384−1390.
(32) Serjeant, E. P.; Dempsey, B. *Ionisation constants of organic acids in aqueous solution*; Pergamon Press: Oxford, 1979.
(33) Widrig, C. A.; Chung, C.; Porter, M. D. *J. Electroanal. Chem. Interfacial Electrochem.* **1991**, *310*, 335−359.
(34) Byloos, M.; Al-Maznai, H.; Morin, M. *J. Phys. Chem. B* **2001**, *105*, 5900−5905.
(35) Muglali, M. I.; Erbe, A.; Chen, Y.; Barth, C.; Koelsch, P.; Rohwerder, M. *Electrochim. Acta* **2013**, *90*, 17.
(36) Srisombat, L.; Jamison, A. C.; Lee, T. R. *Colloids Surf., A* **2011**, *390*, 1−19.
(37) Wang, Q.; Li, N. *Electroanalysis* **2001**, *13*, 1375−1377.
(38) Socrates, G. *Infrared and Raman characteristic group frequencies: tables and charts*; John Wiley & Sons: New York, 2004.
(39) Swoboda, A.; Kunze, G. *Clays Clay Miner.* **1964**, *13*, 277−288.
(40) Liu, J. Self-assembled Monolayers of Functional Group-terminated Molecules on Au. Ph.D. Dissertation, Ruhr-Universität Bochum, 2010
(41) Yang, W.-h.; Li, W.-w.; Dou, H.-j.; Sun, K. *Mater. Lett.* **2008**, *62*, 2564−2566.
(42) Cukier, R. I.; Nocera, D. G. *Annu. Rev. Phys. Chem.* **1998**, *49*, 337−369.
(43) Weinberg, D. R.; Gagliardi, C. J.; Hull, J. F.; Murphy, C. F.; Kent, C. A.; Westlake, B. C.; Paul, A.; Ess, D. H.; McCafferty, D. G.; Meyer, T. J. *Chem. Rev.* **2012**, *112*, 4016−4093.
(44) Reece, S. Y.; Hodgkiss, J. M.; Stubbe, J.; Nocera, D. G. *Philos. Trans. R. Soc., B* **2006**, *361*, 1351−1364.
(45) Xiao, Y.; Patolsky, F.; Katz, E.; Hainfeld, J. F.; Willner, I. *Science* **2003**, *299*, 1877−1881.
(46) Mano, N.; Fernandez, J. L.; Kim, Y.; Shin, W.; Bard, A. J.; Heller, A. *J. Am. Chem. Soc.* **2003**, *125*, 15290−15291.
(47) Heller, A. *J. Phys. Chem.* **1992**, *96*, 3579−3587.
(48) Sirés, I.; Delucchi, M.; Panizza, M.; Ricotti, R.; Cerisola, G. *J. Appl. Electrochem.* **2009**, *39*, 2275.
(49) Fernández, J. L.; Mano, N.; Heller, A.; Bard, A. J. *Angew. Chem., Int. Ed.* **2004**, *43*, 6355−6357.
(50) Keith, J. A.; Carter, E. A. *J. Am. Chem. Soc.* **2012**, *134*, 7580−7583.
(51) Keith, J. A.; Carter, E. A. *Chem. Sci.* **2013**, *4*, 1490−1496.
(52) Keith, J. A.; Carter, E. A. *J. Phys. Chem. Lett.* **2013**, *4*, 4058−4063.
(53) Ertem, M. Z.; Konezny, S. J.; Araujo, C. M.; Batista, V. S. *J. Phys. Chem. Lett.* **2013**, *4*, 745−748.
(54) Li, T. T. T.; Weaver, M. J. *J. Am. Chem. Soc.* **1984**, *106*, 6107−6108.
(55) Feaster, J. Understanding Selectivity of Carbon Dioxide Reduction to Carbon Monoxide and Formic Acid on Sn Electrodes. PRiME 2016/230th ECS Meeting, October 2−7, 2016.
(56) Zhu, W.; Zhang, Y.-J.; Zhang, H.; Lv, H.; Li, Q.; Michalsky, R.; Peterson, A. A.; Sun, S. *J. Am. Chem. Soc.* **2014**, *136*, 16132−16135.
(57) Chen, Y.; Li, C. W.; Kanan, M. W. *J. Am. Chem. Soc.* **2012**, *134*, 19969−19972.
(58) Vaidhyanathan, R.; Iremonger, S. S.; Shimizu, G. K. H.; Boyd, P. G.; Alavi, S.; Woo, T. K. *Science* **2010**, *330*, 650−653.
(59) Rouhana, L. L.; Moussallem, M. D.; Schlenoff, J. B. *J. Am. Chem. Soc.* **2011**, *133*, 16080−16091.
(60) Buck, M.; Grunze, M.; Eisert, F.; Fischer, J. *J. Vac. Sci. Technol., A* **1992**, *10*, 926−929.
(61) Martínez, L.; Carrascosa, L. G.; Huttel, Y.; Lechuga, L. M.; Román, E. *Phys. Chem. Chem. Phys.* **2010**, *12*, 3301−3308.
(62) Manolova, M.; Ivanova, V.; Kolb, D. M.; Boyen, H. G.; Ziemann, P.; Büttner, M.; Romanyuk, A.; Oelhafen, P. *Surf. Sci.* **2005**, *590*, 146−153.
(63) Kim, S. K.; Zhang, Y.-J.; Bergstrom, H.; Michalsky, R.; Peterson, A. *ACS Catal.* **2016**, *6*, 2003−2013.
(64) Yan, Y.; Ge, X.; Liu, Z.; Wang, J.-Y.; Lee, J.-M.; Wang, X. *Nanoscale* **2013**, *5*, 7768−7771.
(65) Miller, F. A.; Wilkins, C. H. *Anal. Chem.* **1952**, *24*, 1253−1294.

DOI: 10.1021/jacs.6b11023
J. Am. Chem. Soc. 2017, 139, 3399−3405